Journal of South American Earth Sciences 119 (2022) 103995

Contents lists available at ScienceDirect

Journal of South American Earth Sciences

journal homepage: www.elsevier.com/locate/jsames

Optimization of local scale seismic networks applied to geothermal fields. The case of the Acoculco caldera, Mexico

Leonarda I. Esquivel-Mendiola [a,*], Marco Calò [b], Anna Tramelli [c], Angel Figueroa-Soto [d]

[a] Posgrado en Ciencias de la Tierra, Universidad Nacional Autónoma de México, Cd. Universitaria, Mexico City, Mexico
[b] Instituto de Geofísica, Universidad Nacional Autónoma de México, Cd. Universitaria, Mexico City, Mexico
[c] Istituto Nazionale di Geofisica e Vulcanologia, Sezione di Napoli, Osservatorio Vesuviano, Via Diocleziano 328, 80124, Napoli, Italy
[d] Instituto de Investigaciones en Ciencias de La Tierra (CONACyT-INICIT), Universidad Michoacana de San Nicolás de Hidalgo, 58000, Morelia, Michoacán, Mexico

ARTICLE INFO

Keywords:
Seismic network optimization
Seismic monitoring
Acoculco geothermal field
Seismic noise level
Topographic gradient
H/V ratio

ABSTRACT

The exploitation of a geothermal field can be accompanied by both natural and induced seismicity. Hence the installation of a seismic network suitable for also locating low-magnitude earthquakes, is of great interest for geothermal development, especially for monitoring the activity related to the injection or production.

Most of the aspects that affect the location of earthquakes are data quality and phase picking, the inverse method chosen to solve the problem, the velocity model, and the seismic network configuration. We focus on the optimization of network configuration and the reduction of the location error is one of the alternatives to finding optimal station positions. Here we propose an improvement of the D-OPTIMAL algorithm (Tramelli et al., 2013) that tries and find optimal station positions minimizing the amount of the error ellipsoid of the event location using the D-criterion. This algorithm is computationally efficient and easy to be implemented. In this version, we also introduced the possibility to account for several prior information that is generally available when implementing a monitoring site permanently or temporarily. These a priori parameters introduced are: i) three-dimensional seismic velocity models, ii) seismic noise levels, iii) topographic gradient, and iv) H/V ratio values. The last three parameters are introduced in the station position selection using a weighted system scheme.

We applied this methodology to the Acoculco geothermal field (Mexico) where an injection test was planned and executed in 2021. The comparison between the network defined using the standard approach, which considers a 1D velocity model and the installation costs, and this improved version shows the importance of introducing a priori information during the selection of the network. Installation sites showed better distribution in the region, resulting in an overall increase in the sensitivity and a decreasing of the error location estimation in the target region.

The methodology presented here is easy to apply to other study cases such as active volcanoes, anthropogenic activities, or other kinds of location studies at local scale.

1. Introduction

Production activities in a geothermal field can be affected by both natural and induced seismicity (e.g., Gaucher et al., 2015; Schoenball et al., 2010, 2013; Toledo et al., 2020). Geothermal fluid extraction and injection cause pressure variations generating changes in the property of the medium that may trigger or induce seismic activity. Although most of these events are low in magnitude (Mukuhira et al., 2013; Urban and Lermo, 2017), induced events large enough to be felt by the population are an undesirable possible result of the geothermal exploitation operations (Buijze et al., 2019). The reliable monitoring and location of the seismic activity in a geothermal field is then a key factor for hazard assessment. Hence an optimal planning of a seismic network is of great interest for geothermal development.

Seismic network improvement has been approached from different perspectives and several authors used different approaches. The most common methods contemplate: i) computation of the magnitude of completeness (*Mc*) and assessment of the spatial distribution of the

* Corresponding author.
E-mail addresses: leoesquivel@igeofisica.unam.mx (L.I. Esquivel-Mendiola), calo@igeofisica.unam.mx (M. Calò), anna.tramelli@ingv.it (A. Tramelli), angfsoto@gmail.com (A. Figueroa-Soto).

https://doi.org/10.1016/j.jsames.2022.103995
Received 28 April 2022; Received in revised form 16 August 2022; Accepted 18 August 2022
Available online 28 August 2022

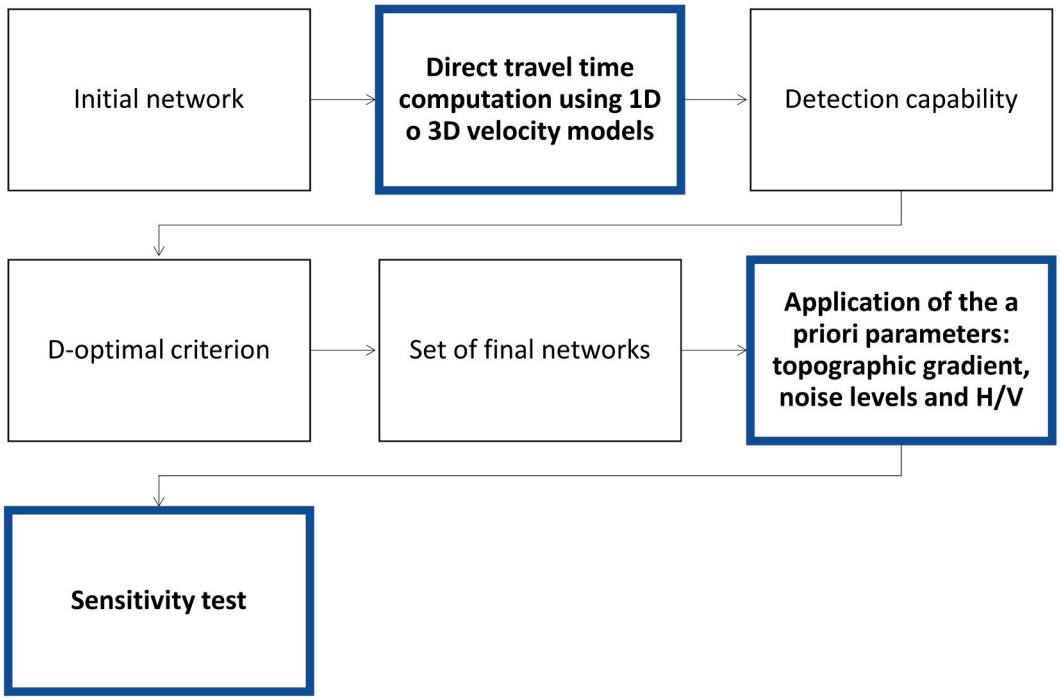

Fig. 1. Workflow of the optimization of a seismic network. Blue-bold rectangles are the steps added with respect to the procedure of Tramelli et al. (2013).

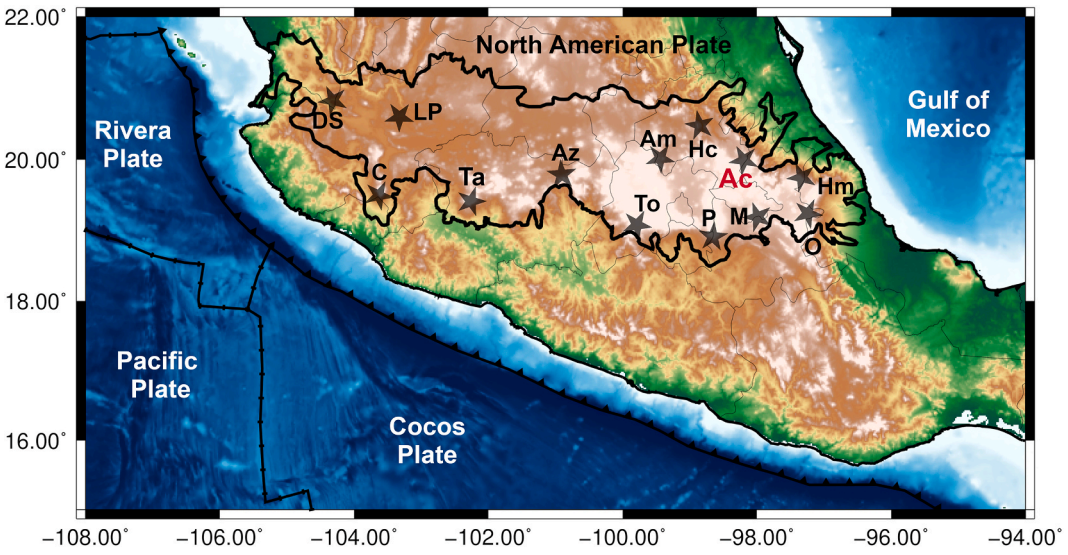

Fig. 2. Tectonic setting of Mexico. Location of the Trans-Mexican Volcanic Belt (TMVB) is marked with a black bold line. Main active volcanoes and geothermal sites of interest located inside the TMVB are: Domo San Pedro (DS), La Primavera (LP), Fuego de Colima (C), Tancítaro (Ta), Los Azufres (Az), Amealco (Am), Huichapan (Hc), Nevado de Toluca (To), Popocatépetl (P), Malinche (M), Pico de Orizaba (O) y Humeros (Hm). A black star and red letters mark the location of the Acoculco Caldera (AC) (modified from Avellán et al., 2020).

location error (e.g., the Seismic Network Evaluation through Simulation - SNES, Mahani et al., 2016; D'Alessandro et al., 2011b, 2013, 2014); ii) location of the seismic events using a combination of random station locations applying probabilistic methods (e.g., Monte Carlo) to decrease the location errors (e.g., Bondár et al., 2004); iii) correction of teleseismic travel times (e.g., Myers and Schultz, 2000); iv) mapping the expected location errors and assessment of the lowest magnitude of events that the seismic network can detect (e.g., Stabile et al., 2013; De Landro et al., 2020); and v) employment of the D-criterion to identify an optimal seismic network configuration to decrease the location error (e.g., Steinberg and Rabinowitz, 2003). In this last case, the network optimization can contemplate genetic algorithm (e.g., Bartal et al., 2000), simulated annealing (e.g., Hardt and Scherbaum, 1994; Kraft et al., 2013), or Bayesian techniques (e.g., Coles and Curtis, 2011; Tramelli et al., 2013).

In any case, seismic monitoring depends on four main aspects: i) seismic network geometry, ii) sensitivity to detect targeted seismicity, iii) location method, and iv) knowledge of the velocity model.

In this study, we focus on the seismic network geometry improvement by proposing an updated version of the algorithm D-Optimal proposed by Tramelli et al. (2013) that tries and finds the optimal station positions minimizing the volume of the error ellipsoid of the location for synthetic earthquakes using the D-criterion (Rabinowitz and Steinberg, 1990, 2000; Steinberg and Rabinowitz, 2003). This algorithm is

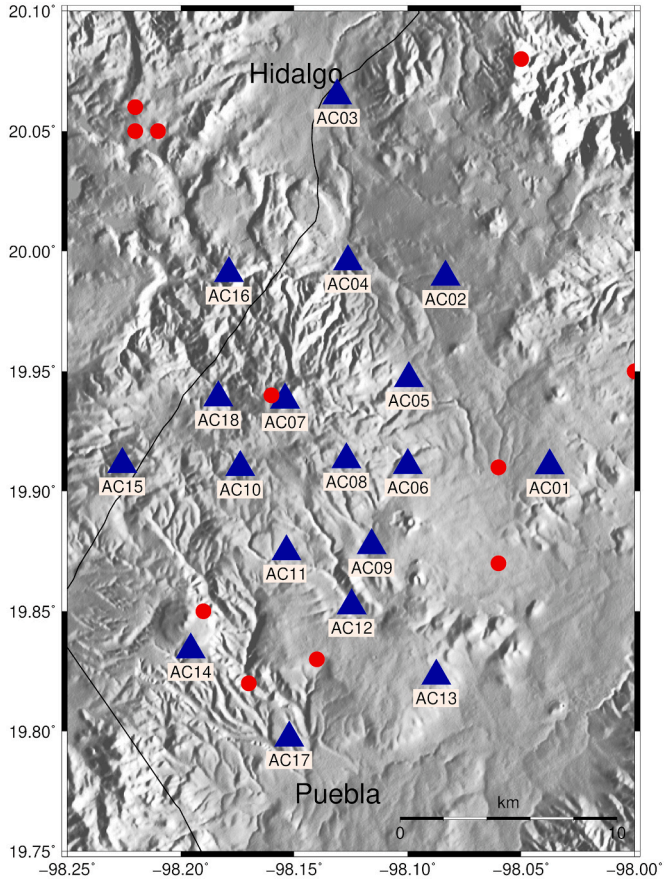

Fig. 3. Temporal seismic network installed in 2018 at the Acoculco volcanic complex (blue triangles) and local seismicity located within 25 km of the study area (red dots).

particularly convenient because of its easy implementation, computationally efficient, and is enough reliable in finding absolute minima of the function error (Kijko, 1977; Rabinowitz and Steinberg, 1990; Mitchell, 2000; Tramelli et al., 2013; Toledo et al., 2020). The optimization process accounts for every station combination based on permutation of preestablished sites using the Monte Carlo method and covariance to restrict the ellipsoid error of the hypocenter location.

In this version of the program, we improved the procedure by considering several prior information such as maps of seismic noise levels, amplitude picks obtained from *H/V* analysis and three-dimensional seismic models of the study region. This information is usually produced during the exploration stage of a geothermal site and available before an injection test. Additionally, we introduced the topographic gradient as a selection parameter to allow better planning of the installation campaigns in regions with rugged topography.

We applied the methodology to the Acoculco geothermal field (Mexico) where an injection test was carried out in June 2021, and an intense exploration campaign was performed between 2018 and 2020 in the framework of the Mexican European consortium GEMex (Cooperation in Geothermal energy research Europe-Mexico).

A comparison between the standard approach and this updated version shows the importance to use different prior parameters for a more suitable optimization of the local scale seismic networks, including the topography of the region that allowed to simplify the logistic of the installation.

2. Seismic network optimization

The approach proposed by Tramelli et al. (2013) finds a suite of possible optimal networks starting from an initial hypothetical set of N possible sites and computes the synthetic amplitude of a hypothetical earthquake to determine the detection capability for each station. Source amplitude is computed using the source parameters expected for an event that may occur in the analyzed region (i.e., stress drop ($\Delta\sigma$), hypocenter coordinates, and moment magnitude (M_W) using the Brune model (Brune, 1970). Additionally, a reference model, with mean shear wave velocity (V_S), density (ρ), and quality factor (Q), is used to account for the attenuation properties to properly calculate the signal amplitude at each hypothetical station position. Finally, the Signal Noise to Ratio (SNR) is computed for each site where a station could be installed.

Monte Carlo method is then used to construct random stations combinations from M available stations situated in N possible sites. For each configuration, the algorithm computes the covariance matrix and applies the D-criterion (Rabinowitz and Steinberg, 1990, 2000) to find the optimal configuration. The D-Optimal algorithm uses the confidence ellipsoid error as a parameter for finding the optimal network configuration. This parameter is used to optimize the geometry of seismic networks because it provides a good approximation of the real location error (e.g., D'Alessandro et al., 2011a, 2011b; Tramelli et al., 2013; Toledo et al., 2020). The minimization of the volume of the error ellipsoid is achieved through iterative changes in the station positions.

The standard version of the D-Optimal algorithm computes the travel times between events and stations using 1D velocity models of the P and S waves and it can read travel times computed from the 3D velocity model in an external process. In this version, we incorporated into the algorithm the direct computation of the travel times using 3D seismic velocity models using the pseudo-bending method. This was achieved by extracting the subroutines from the well-established tomographic code Simul2000 (Thurber, 1993; Eberhart-Phillips, 1993; Thurber and Eberhart-Phillips, 1999) and incorporating them into the code. The other parameters that could influence the selection of a network are instead incorporated using a weighting system applied a posteriori.

The procedure of Tramelli et al. (2013) has then been modified with a workflow (Fig. 1) that contemplates the following steps: i) computing of the travel times using 1D or 3D velocity models, ii) computation of the detection capability, iii) applying the D-Optimal criterion to obtain the corresponding determinant values (D) of potential final networks, iv) reduction of the final networks space by applying a weighting system of the priori parameters to the potential networks with the highest determinant, and v) estimation of the sensitivity for the best configurations that meet the a priori parameters.

3. A priori parameters

In our procedure, the a priori parameters were added as a weight system that helps to choose between a set of configurations with similar D values, penalizing the selection of networks whose installation sites are characterized by high topographic gradient values, high noise levels, and low amplification factors (H/V values).

3.1. Topographic gradient

Instrument installation on a strong slope could be difficult and may increase the installation and maintenance costs. In addition, the recorded seismic signal would be affected by topographical effects. Therefore, the topography of a region is an important characteristic to consider during the planning of an installation campaign.

We used the topographic gradient (TG) as a parameter to avoid sites where accessibility can be difficult. The topographic gradient for the entire region was computed as

$$TG = \sqrt{G_{NS}^2 + G_{EW}^2} \quad (1)$$

where G_{NS} is the gradient in the North-South direction, and G_{EW} is the gradient in the East-West one. For each possible site, we assign a topo-

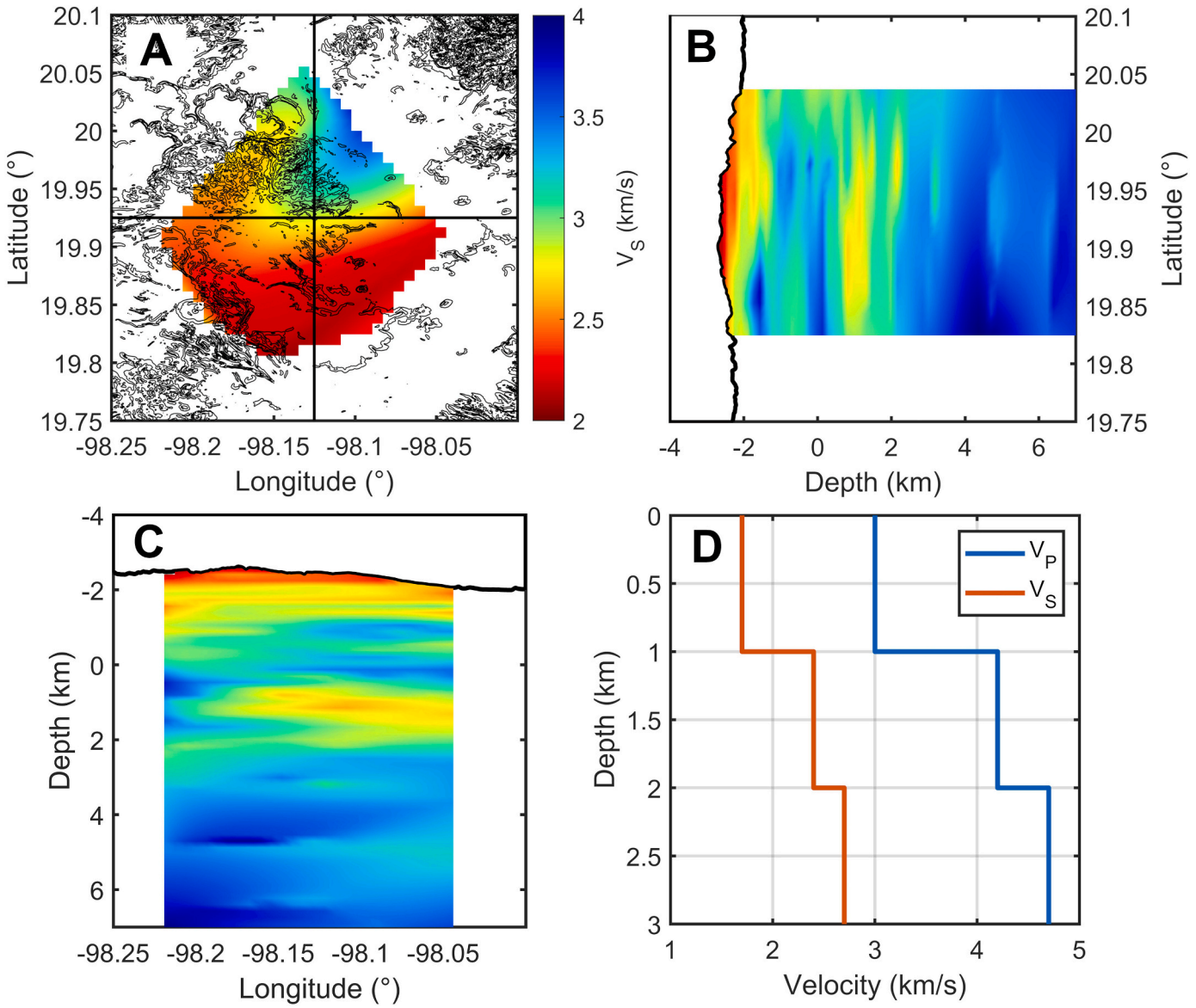

Fig. 4. Three-dimensional S wave velocity model (Vs) of Acoculco geothermal field. A) Horizontal section of the Vs model at 1 km a.s.l., B), N–S, and C) E-W vertical sections. (d) Mean layered one-dimensional velocity model of P and S waves was used to locate the seismicity and to perform the tests described in the main text. (Modified from Maldonado-Hernández et al., 2019).

graphic gradient calculated as the mean value on a radius of 150 m from the site. Finally, we compute a normalized average topographic gradient value for each seismic network with respect to the maximum mean value of the topographic gradient. This mean value is considered as a representative gradient value of the network and used as a weighting factor for the site selection.

3.2. Noise levels

Root Mean Square amplitude (RMS) or Power Spectral Density (PSD) are usually used to characterize the seismic noise level in a site. In our procedure, we generate maps of noise levels at different frequency bands by interpolating the PSD calculated in sites within a grid using the cube interpolation technique. Subsequentially, for each potential network, we calculate the corresponding mean noise level as the average of the values at each station composing the network for the bandwidth of interest. Finally, the weights relative to the noise level of a network are obtained by normalizing the vector of the mean values with respect to the maximum mean noise level.

3.3. H/V ratio

The H/V ratio is related to the amplification power of a particular site and depends on its specific geological and topographical characteristics. The larger the H/V, the stronger the amplification of the shear waves is. Although high H/V in a site could make it more difficult to identify the P wave arrivals, the fact that the S waves are amplified would ensure better detection of the event because the latter is almost always more energetic than the first ones. Then, amplitude increase is estimated for various frequency ranges and considered as a parameter that can facilitate microseismicity detection when the amplification of the S waves is high in the frequency range of interest.

Similarly, as in the case of the noise level, the weights of the H/V ratio are considered as normalized mean values with respect to the maximum value calculated on cubic-interpolated maps for each possible seismic network.

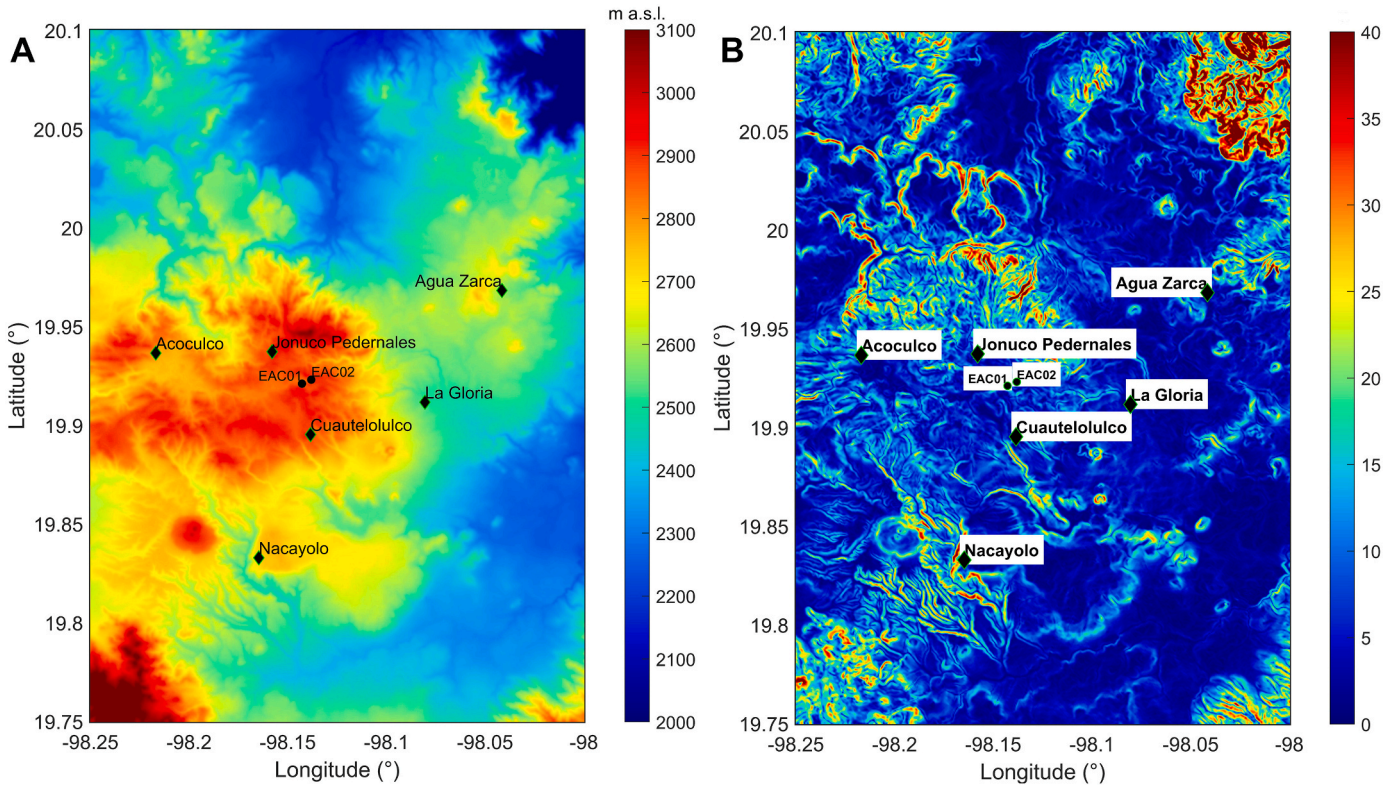

Fig. 5. Topography (A) and topographic gradient (B) of the Acoculco volcanic complex. Principal towns are indicated with black diamonds. Boreholes EAC01 and EAC02 are indicated with black circles.

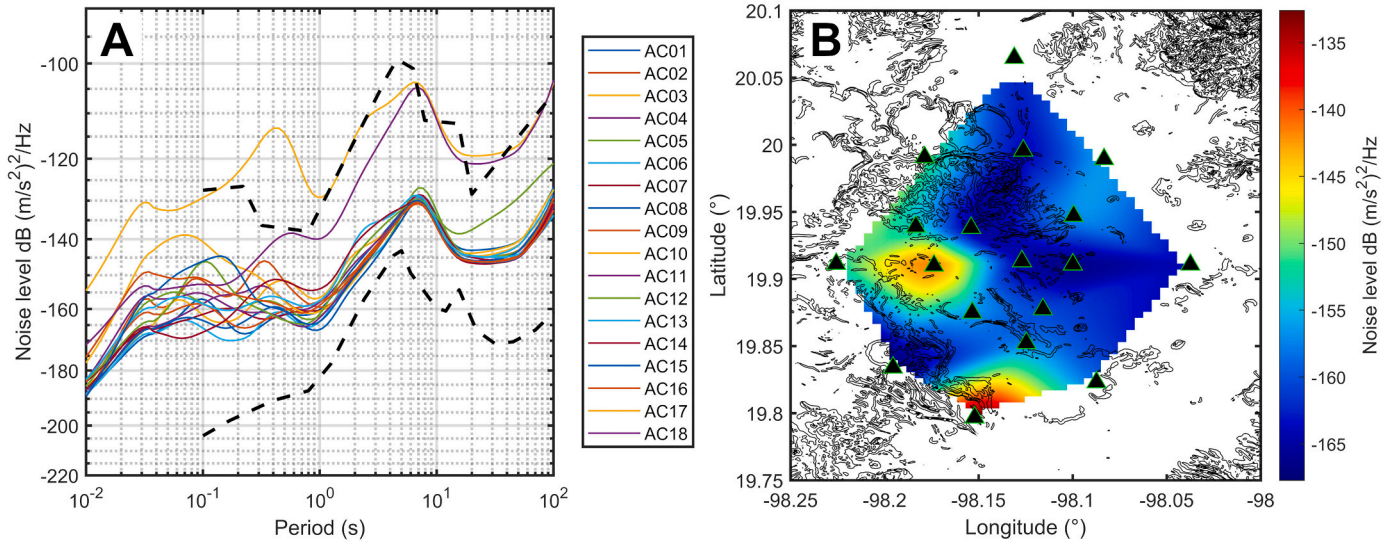

Fig. 6. (A) Median of the PSD calculated from September 2018 to April 2019 at the 18 temporary stations installed. (B) Noise level map in the frequency range of 10–40 Hz; black triangles are station locations of the temporary network.

3.4. Ponderation system

The ponderation system establishes how the a priori information is accounted for during the selection of an optimal seismic network. We considered the determinant value as the main parameter because the aim of the optimization is the resolving power of the network. For this reason, we organize the networks proposed by D-OPTIMAL algorithm in decreasing order as a function of D. High values of TG and noise levels are unfavored parameters, we then organize them in increasing order. Conversely, H/V values are organized in decreasing order because high values are considered a parameter in favor of the networks considered. We used the organized vectors, in ascending or descending order, obtaining the potential networks ordered as a function of the a priori parameters. We then compare the ordered vectors to find those configurations that maximize or minimize the a priori parameters. In this way, the optimal networks are selected depending on if they are associated with high D, low TG, low noise level, and high H/V ratio.

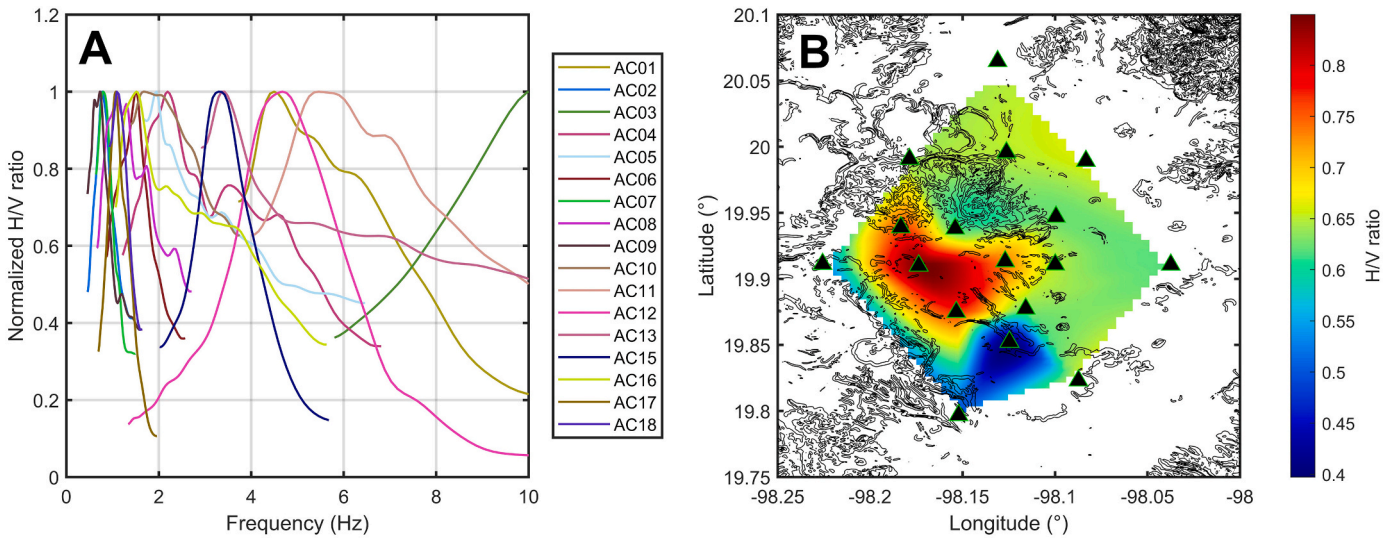

Fig. 7. (A) Normalized H/V curves estimated by Ibarra-Bustos (2019) for the temporal network installed between May 2018 to July 2019 (B) Map of the H/V ratio computed using the H/V ratio values. Black triangles are the station locations of the temporary network.

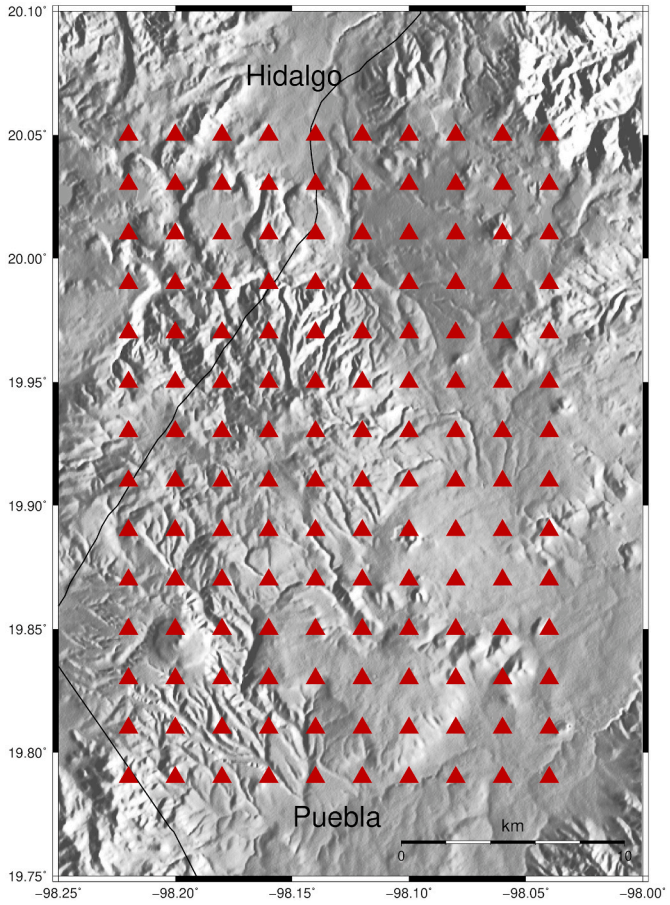

Fig. 8. Location of 140 station sites representative of the 2378 possible sites available for the virtual network. The spacing of the initial virtual station sites is 500 m.

3.5. Sensitivity test

Once some of the a priori parameters are introduced to the procedure, we can obtain a reduced set of seismic networks that maximizes determinant value and H/V ratio and minimizes topographic gradient and noise levels. The procedure allows setting the number of the potential configurations that will be admitted for further analyses. Finally, the choice of the best seismic configuration is obtained by calculating the network sensitivity.

In this case, we calculate the network sensitivity using the Sensitivity Estimate of a Seismic Network algorithm (SENSI) developed by Tramelli et al. (2015). SENSI computes synthetic seismic signals using the Brune model (Brune, 1970) for a source point as a function of the magnitude, stress drop, shear wave velocity, density, and minimum number of stations to detection or location. The minimum magnitude event is calculated for each source point distributed in a regular grid (Orazi et al., 2013; Tramelli et al., 2015) considering the signal to noise ratio.

4. Application to Acoculco geothermal field (Puebla, Méx.)

4.1. Geological settings

Acoculco caldera is located in the eastern most part of the Trans Mexican Volcanic Belt (TMVB) (Fig. 2). Rhyolites-dacites-andesites-basaltic and rhyolites-dacites tuffs from 1.4 to 0.24 Ma characterize the main volcanic rock composition (López-Hernández and Castillo-Hernández, 1997). Eruptive chronology has been grouped into four main eruptive phases: syn-caldera, early post-caldera, late post-caldera, and extra-caldera (Avellán et al. 2020). The latter began around 2.7 Ma with the dispersion of andesitic ignimbrite followed by the collapse of the magma chamber. The volcanic complex is affected by two regional stress regimes with NE-SW and NW-SE orientations (López-Hernández and Castillo-Hernández, 1997; López-Hernández et al., 2009). Three-dimensional heat flow modeling obtained using an estimated Curie temperature isotherm suggests the presence of a heat source of at least 750 °C between 3100 m and 3400 m of depth (Guerrero-Martínez et al., 2020).

Since the early nineties, because of the intense hydrothermal manifestations, acid springs, and gas discharges present near the Acoculco caldera, the Mexican Federal Electricity Commission (CFE) started several exploration activities and in 1995 the first exploratory borehole (EAC01) was drilled to a depth of 1810 m near to Los Azufres, a hydrothermal manifestation with many gas emissions. In 2008 a second borehole (EAC02) was drilled reaching a depth of 1900 m confirming high temperatures in depth. However, the low permeability found at these depths discouraged the development of conventional high enthalpy geothermal systems (Kruszewski et al., 2021; López-Hernández et al., 2009; Bolós et al., 2022).

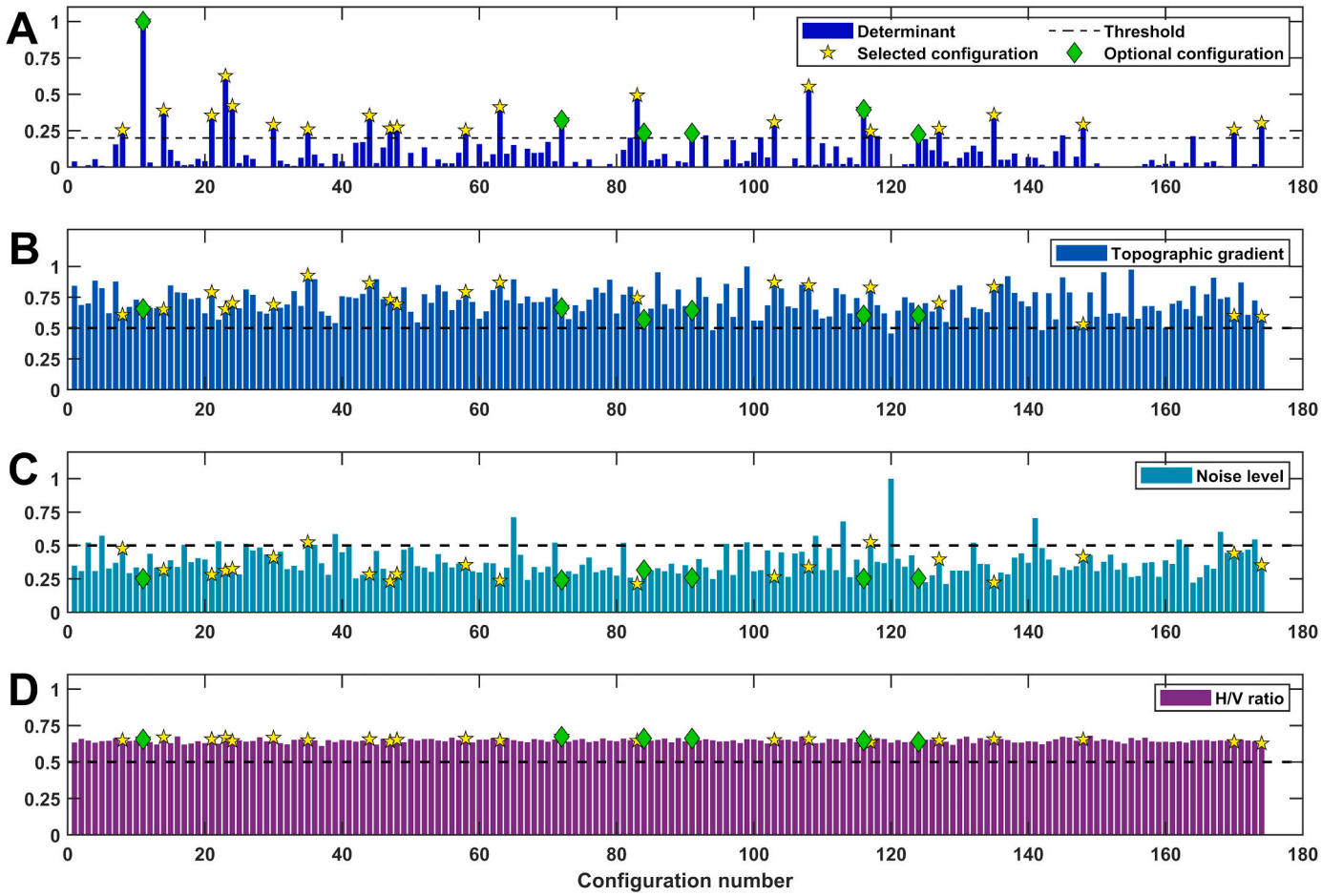

Fig. 9. Normalized determinants (A), topographic gradients (B), noise levels (C), and H/V ratios (D) for different seismic network configurations using the 1D velocity model. Dashed lines are the thresholds or reference values used for the network selection. Yellow stars are the configurations that meet the threshold parameters whereas green diamonds are the six best optimal seismic networks selected.

A hydraulic stimulation of the borehole EAC01 was planned in 2018 and executed in 2021. Different scenarios such as hydraulic fractures, fracture network stimulation, fault zone reactivation, and a combination of the previous scenarios have been planned with the integration of geological, geophysical, and geochemical information (GEMex W.P. 7.1, 2020). Finally, a fracture network stimulation was tested by injecting fluids on July 14, 2021, as a final activity within the GEMex project.

4.2. Seismicity and velocity models

Acoculco geothermal field had a limited monitoring activity. Between 1995 and 2018 only a temporal network of seven sensors (4 velocimeters and 3 accelerometers) was deployed for four months in 2004 (Lermo et al., 2009). No local seismicity was detected during this period and 30 regional seismic events were used to build a preliminary 1D velocity model of the region using the Spatial Autocorrelation method (SPAC).

Recently, as part of Work Project 5.2 of GEMex, 18 broadband seismic stations were installed in the Acoculco complex (Fig. 3) and recorded from May 2018 to July 2019. The network was specifically designed to apply ambient noise and SPAC techniques. Maldonado-Hernández et al. (2019) obtained a three-dimensional velocity model of the S waves (Fig. 4) using the first order and overtones of the group velocities extracted employing the ambient noise cross-correlation method. The model is characterized by the presence of strong lateral heterogeneities and a low velocity zone at depths of 0.5–3 km b.s.l. Additionally, the network recorded 33 local events with magnitude up to 3 and mainly located outside of the caldera rim (Figueroa-Soto et al., in submission). Among these, 11 events are located within 25 km of the study area.

4.3. Topographic gradient

According to the Digital Elevation Model (DEM) provided by the Mexican National Institute of Statistics and Geography (INEGI), Acoculco volcanic complex has a rugged topography (Fig. 5A). Local topography ranges between 2000 and 3100 m a.s.l. over an area of approx. 20×20 km^2. Specifically, the volcanic caldera extends between 2600 to more than 3000 m a.s.l.

The computation of the topographic gradient (Fig. 5B) highlights the shape of the caldera border and the main drainage pattern, which is characterized by strong variations of the slope. Map resolution is 50 m and TG can reach 30–40 in several parts of the mesh corresponding to a slope of about 80%.

4.4. Seismic noise levels

Seismic noise levels were computed using the continuous records of the temporal seismic network (Fig. 3) composed by 18 broadband seismic stations installed from September 2018 to April 2019 (W.P. 5.2, GEMex).

Fig. 6. A shows that the median of the PSD estimated at the stations are within the minimum and maximum levels of the Peterson curves (Peterson, 1993). However, two of them (AC17 and AC18) exhibit

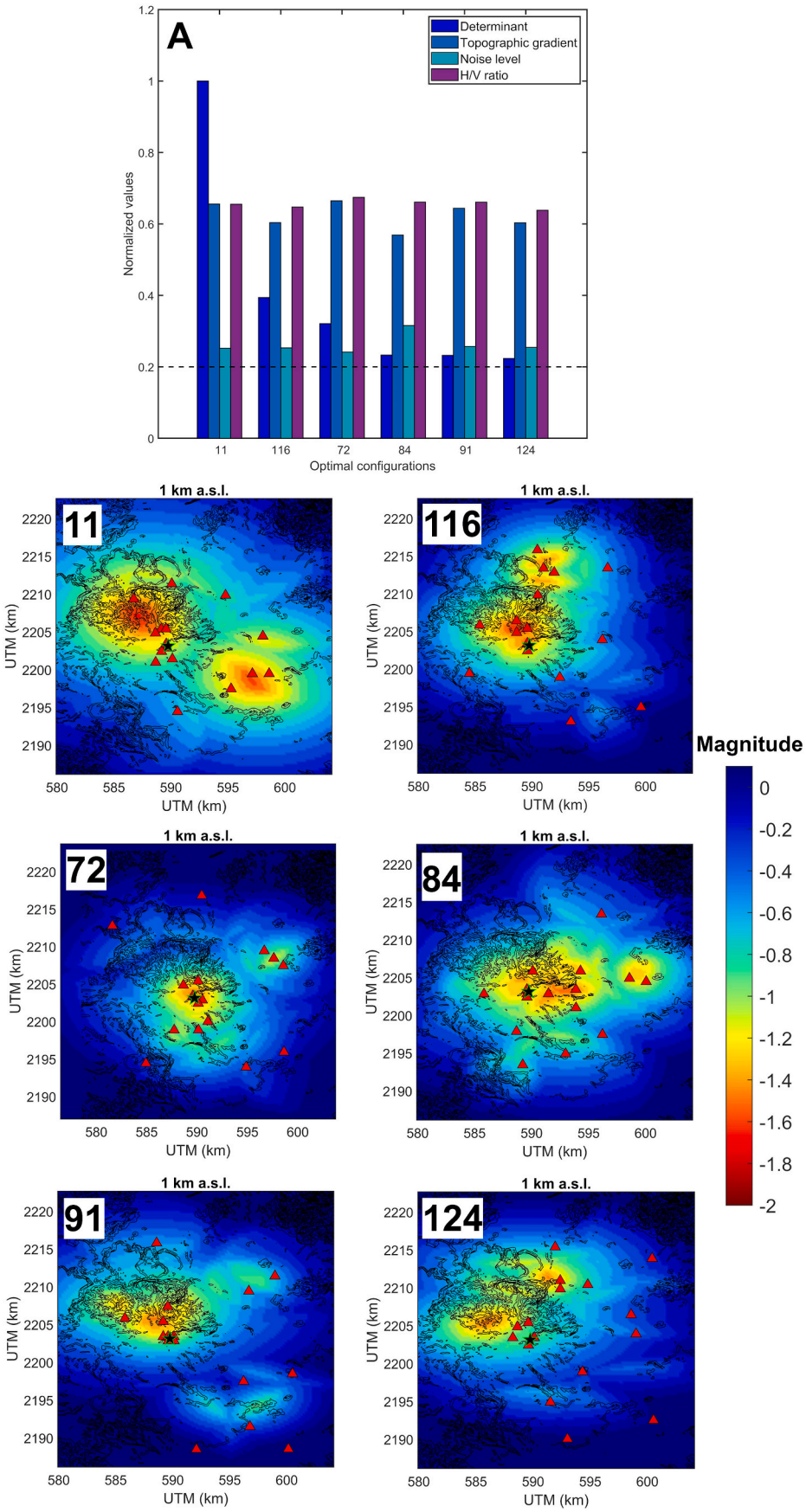

Fig. 10. Top: Histograms of the six seismic networks selected using the 1D velocity model. Bottom: Sensitivity maps at 1 km a.s.l. (approx. 1.8 km of depth). Red triangles are the station locations proposed. Black star is the earthquake position.

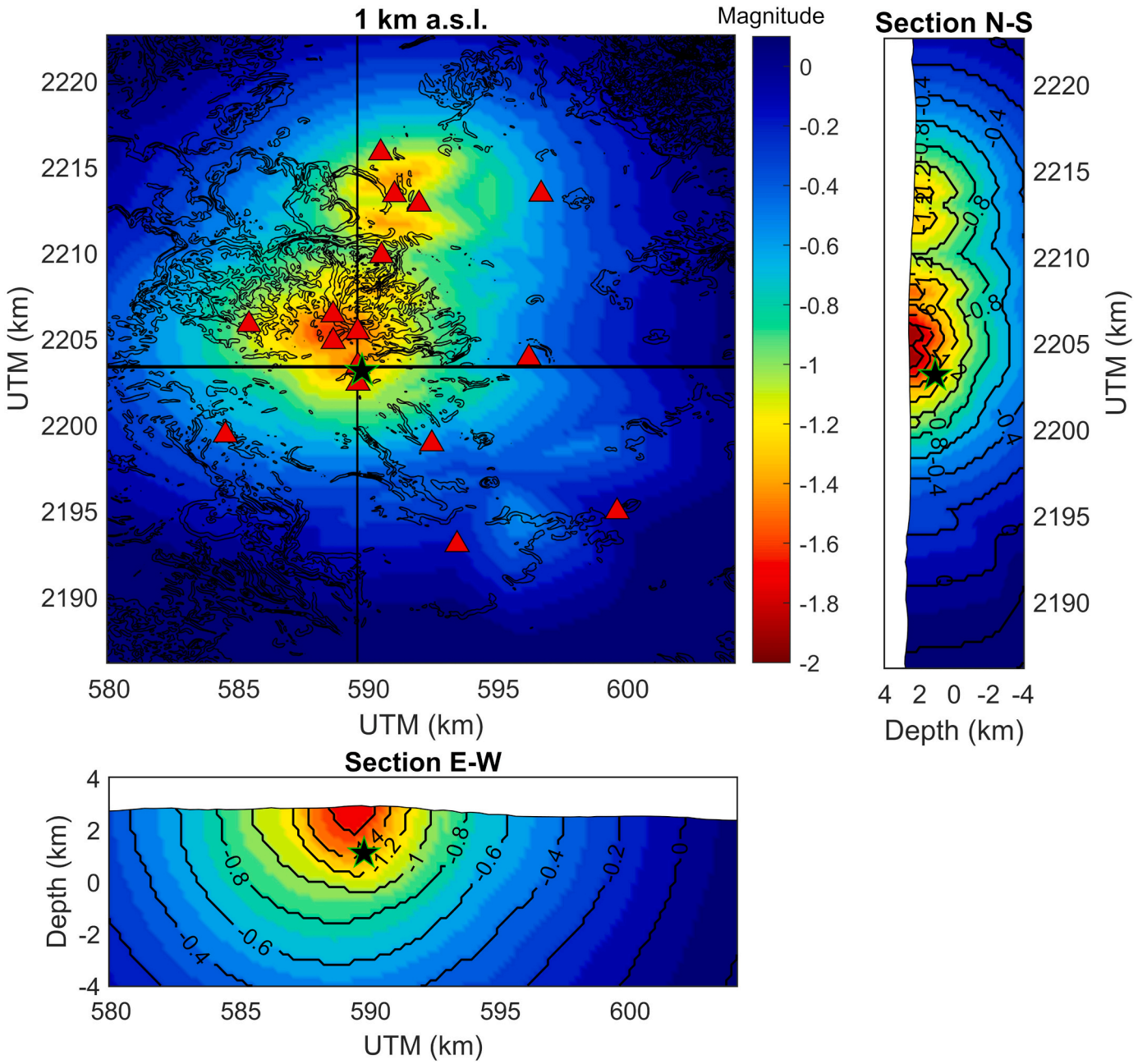

Fig. 11. Sensitivity map for the seismic network numbered 116 at 1.8 km depth (1 km a.s.l.) using the 1D velocity model. The magnitude range capable of being detected is indicated by the color bar, red triangles represent the stations, and the black star the hypocenter. Vertical and horizontal solid lines indicate North-South and East-West sections.

slightly higher levels than the rest of the curves. This is attributed to the vicinity of the stations to the populated regions and to site effects.

Generally, induced seismicity observed in geothermal fields has a small magnitude ($M < 2$; Gupta, H. K., 1992) and exciting mostly high frequency. Thus, we computed the spatial distribution of the mean seismic noise level of the entire geothermal field in the frequency range of 10–40 Hz (Fig. 6B). Map of Fig. 6B shows that the highest values are in the northwest and south regions, where AC17 and AC18 stations are placed.

4.5. H/V values

To estimate this parameter, we used the H/V values computed by Ibarra-Bustos (2019) using the seismic network deployed in 2018 at the Acoculco volcanic complex. A map was computed using a cubic interpolation of the mean values of the normalized H/V curves (Fig. 7A) in the frequency range of 0.1–10 Hz. Although different from the frequency band selected for the seismic noise levels, this is the bandwidth that includes all the maximum amplitudes measured at the stations (Fig. 7A) and where the S waves are better amplified. With this approach even when the curves have maximum H/V ratio values at different frequencies, normalized values guarantee to account for them with the same weight during the map building. Fig. 7B shows the distribution of the mean normalized amplitudes highlighting the presence of low values in the southern region close to AC12, and high amplification values in the western region.

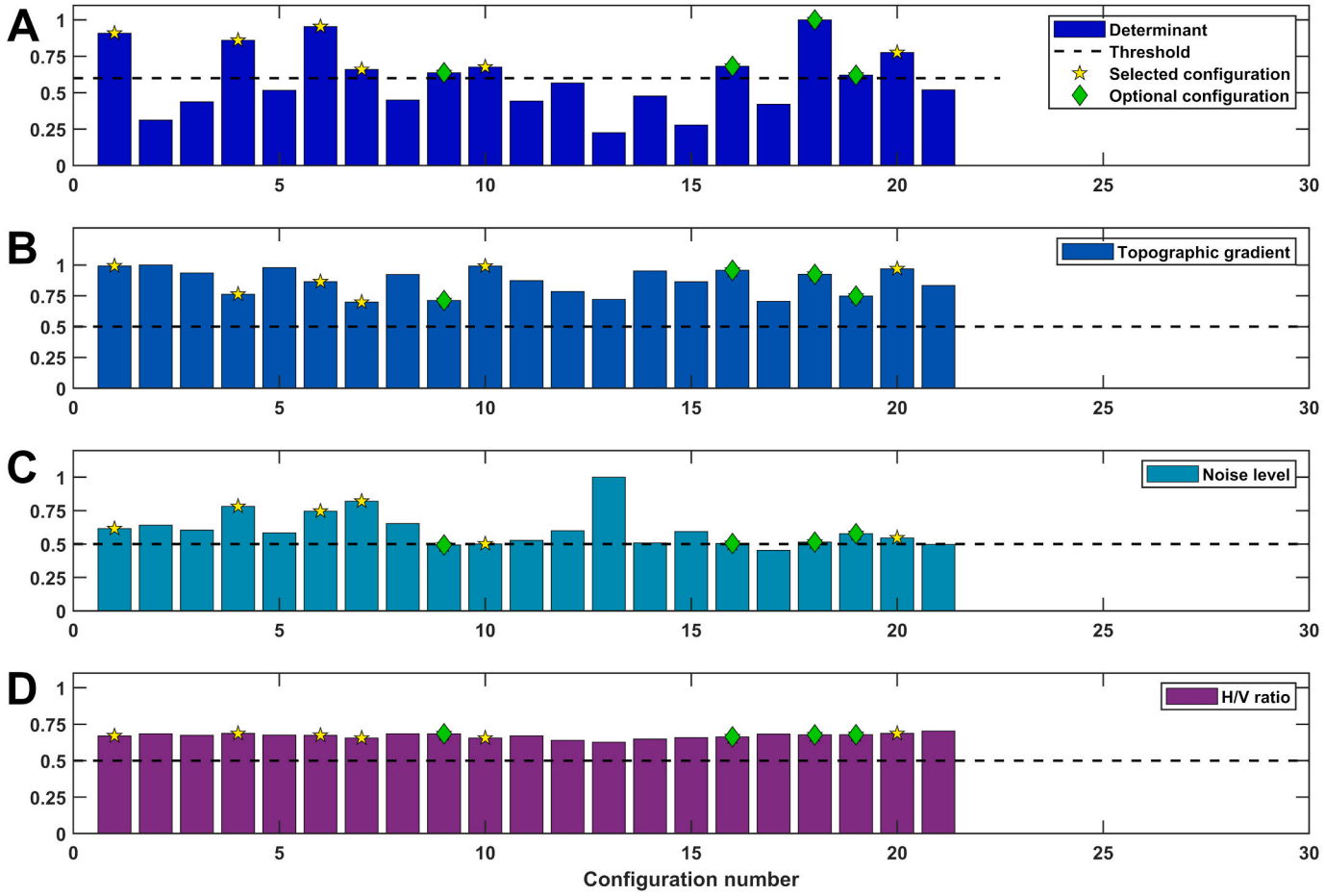

Fig. 12. Normalized determinants (A), topographic gradients (B), noise levels (C), and H/V ratios (D) for different seismic network configurations using the 3D velocity models. Dashed lines are the thresholds or reference values used for the network selection. Yellow stars indicate the configurations that meet the threshold parameters whereas green diamonds are the six best optimal seismic networks selected.

4.6. Optimization network

In order to assess how sensitive is the procedure to the velocity model used in the travel time computation in D-optimal, we applied the whole process using both the 1D reference model and the 3D one. Since the 1D and 3D velocity models proposed by Maldonado-Hernández et al. (2019) are relative to the S waves, the P ones were retrieved using a constant Vp/Vs = 1.6. Subsequently, a grid of 2378 potential station sites is generated, locating them on a regular grid of 20 × 28 km covering the study area with a station spacing of 500 m (Fig. 8). For our analysis, the number of stations available for the potential network is 16 and can be distributed over 2378 possible sites. The determinant and the a priori parameters are then calculated for each potential configuration. Also, we normalized the determinant values to easily identify the seismic network configuration with the best determinant value. The normalization was computed with respect to the maximum determinant value of all potential seismic networks. We set the maximum number of potential final configurations to 6, in order to evaluate the performance of the ponderation system and analyze the event detection capability of more than one network. The sensitivity of the networks was estimated by simulating the occurrence of an event located within the well EAC01 at a depth of 2 km. Since the depth of the wells is 1.9 km, we consider that the expected stimulation would occur at its bottom.

The parameters used to simulate the synthetic event are a mean shear wave velocity of 1.7 km/s (Maldonado-Hernández et al., 2019), a density of 2.4 g/cm^3 (López-Hernández, 2009), a Q = 90 (W.P. 5.2 of GEMex, 2021), and a stress drop of 0.5 MPa. The last one is compatible with the range between 0.01 and 3 MPa of an expected event induced during a hydraulic stimulation (Lengliné et al., 2014). Moreover, we consider only events that can be detected at least three stations with a signal to noise ratio greater than 2.

Results obtained using the travel times calculated on the 1D model together with the normalized values of the determinant, topographic gradient, noise level, and H/V ratio are reported in Fig. 9. The D-Optimal algorithm selected 174 potential networks able to locate events in the region with a determinant average of 0.09. This set can be reduced to 24 potential configurations when considering a D > 0.2 (diamonds and stars in Fig. 9). This set of configurations is further reduced to 6 potential networks when the a priori parameter ponderation is added (diamonds in Fig. 9). The selected configurations reflect the following conditions: 1) D > 0.2, 2) TG > 0.5, 3) noise levels ≤ 0.5, and 4) the highest amplification factors of the H/V values.

Although yellow stars pointed to seismic configurations with D values suitable for the selection of a network, the TG and noise levels resulted in the main a priori parameters that influenced their exclusion due to unfavorable conditions related to logistic and/or noisy locations.

Another relevant aspect resulted in this test, is the low contribution of the H/V in the ponderation system. This is because the calculated average values are almost the same for all the 174 potential configurations.

Fig. 10 reports the parameters of the 6 networks that have been selected and ordered according to the D value together with the other parameters. Therefore, we analyzed the histogram of each seismic configuration, its spatial distribution, and its sensitivity. Since

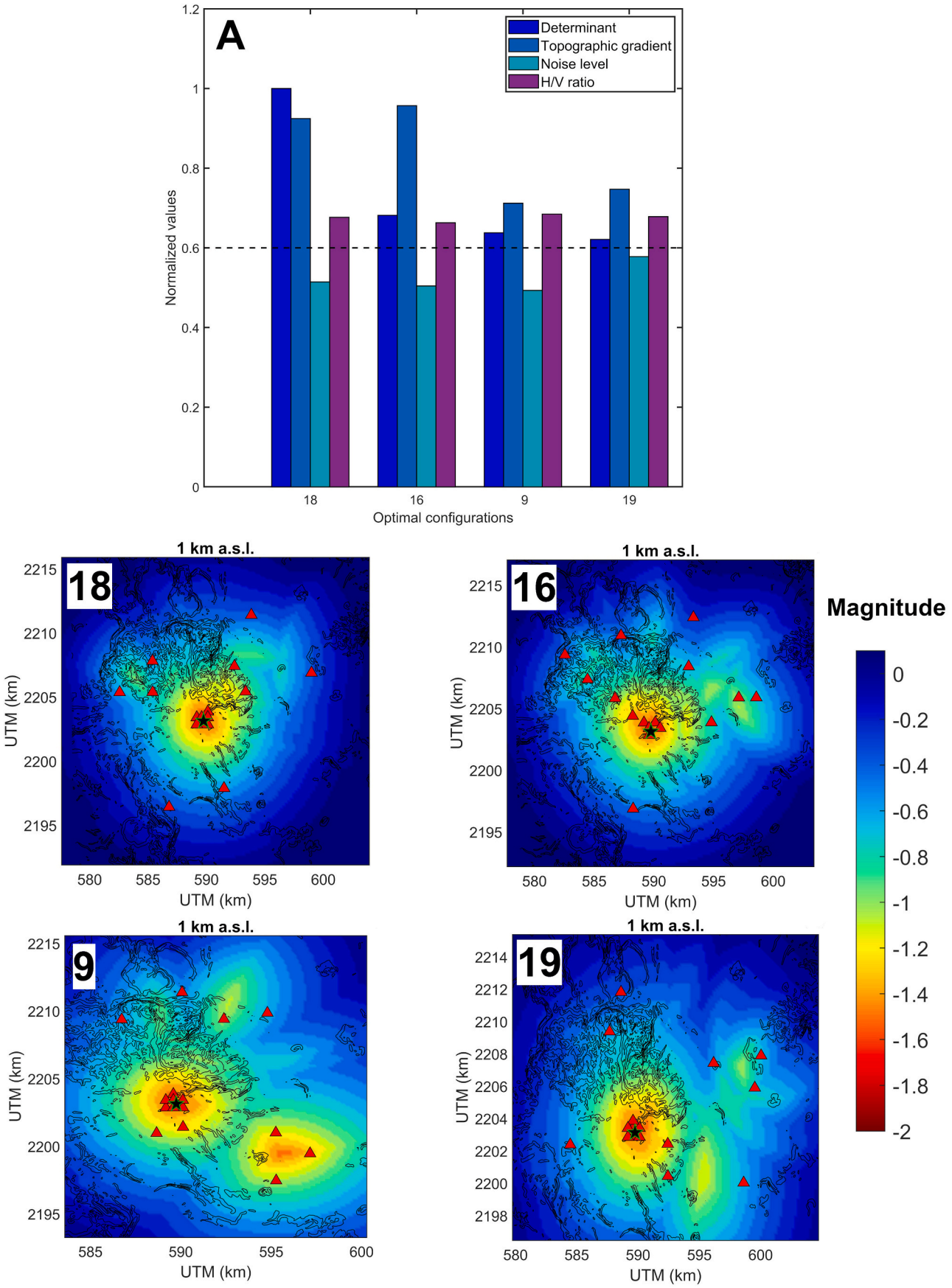

Fig. 13. Histograms of the 4 seismic networks selected as optimal using 3D velocity model at the top. Resolving distribution for each optimal seismic network with stations (red triangles) and hypocenter (black star) at the bottom.

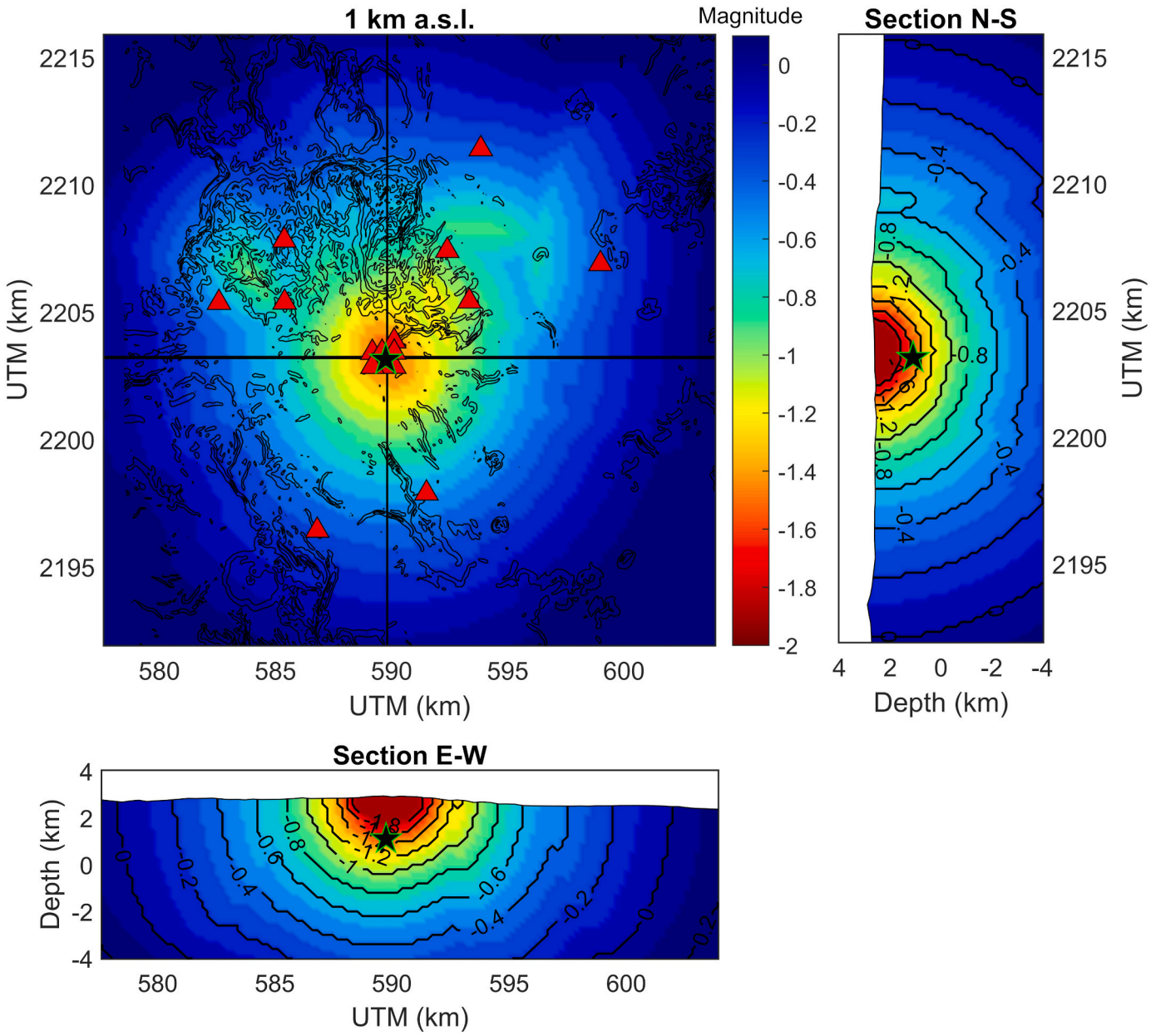

Fig. 14. Sensitivity test for seismic network number 18 at 2 km depth (1 km a.s.l.) using the 3D velocity model. The magnitude range capable of being detected is indicated by the color bar, red triangles represent the stations, and black star the hypocenter. Vertical and horizontal solid lines indicate North-South and East-West sections.

configuration 11, although reports the best values of D, shows a high heterogeneity of the station distribution and sensitivity not centered at the location of the targeted event (marked with the black star in Fig. 10), we discarded it and preferred the network 116 (Fig. 11) which displays a better azimuth coverage and a sensitivity more centered on the target region.

The map at 1 km a.s.l. (i.e., about 1.8 km of depth, Fig. 11) indicates that this kind of configuration offers the largest sensitivity NW of the target region. The North-South vertical section shows the spreading of the sensitivity in the north direction and that, events of magnitude of ~ -1.2 or larger can be detected and located at the targeted depths. The east-west section shows the highest sensitivity concentration near the hypothetical hypocentral zone with a maximum detection power of M ~ -1.7 in the first km of depth.

The same procedure was applied using the modified version of D-OPTIMAL that allows direct travel times computation using 3D velocity models (Fig. 12). In this case, we observed that the possible configurations obtained were only 21. With the threshold of $D > 0.6$, almost 50% of the total are kept and at least 5 of them have normalized determinants greater than 0.75, TG > 0.6, noise level ≥ 0.5, and H/V ≈ 0.6.

Fig. 13 shows the histogram of the 4 best configurations together with their spatial distribution, and their sensitivity at 1.8 km of depth. In this case, we can observe that all the seismic networks selected to produce the greatest sensitivity concentrated in the hypocentral region. However, networks 16, 9, and 19 show low D values and dispersion of the sensitivity in regions different from the one of interest.

Map at 1 km a.s.l. of network 18 (Fig. 14) suggests a good azimuth coverage in the hypocentral area. North-South and East-West sections show that sensitivity is concentrated in the hypocentral volume. On average, events with M ≥ -1.5 can be detected and located at the targeted depths in an area with a diameter of approximately 5 km.

5. Discussions and conclusions

Design of a seismic network is always a difficult task, especially when the targeted seismicity is of low magnitude such as the one expected in operative geothermal power plants. Most of the existing algorithms are designed to find suitable network configurations without considering valuable a priori information that can make the difference in the selection of the best sites (Toledo et al., 2020; Edwards et al., 2015; Baujard et al., 2018). The standard D-OPTIMAL algorithm resulted a performant and flexible tool to optimize the network configuration at the local scale. However, this upgraded version, which allows the direct computation of travel times in 3D models, highlighted how important the lateral heterogeneities of the wavefield are in the planning of the optimized networks. This aspect is often neglected and may lead the operators to potential evaluation errors that may strongly affect the efficiency and the sensitivity of the seismic network.

Seismic noise levels resulted in important information that should be considered to make the a posteriori selection of the possible configurations, demonstrating that a previous campaign aimed at estimating the local fluctuations of this parameter is of great importance for achieving performant networks. Conversely, and surprisingly, H/V resulted without influence on the site selection. This may be attributed to the fact that the range of frequencies in which most of the pick amplitudes were observed fall outside the frequencies expected for the microseismicity (>10 Hz).

Finally, the decision to add the topographic gradient as a constraint for the network selection resulted of great importance to properly planning the logistic of installation. In Acoculco, slopes can reach 80% in several regions making it difficult not only for the installation but also the subsequent maintenance of the sites.

With the approach presented here, further parameters can be easily added to the procedure of the network selection, e.g., geological, and structural maps, phone and telecommunication coverage, route accessibility, etc. All this analysis has the aim to maximize the efficiency of the network lowering the installation and maintenance costs.

For the Acoculco volcanic complex, the sensitivity of the designed network shows that events of magnitude down to −1.1 could be detected and located at depths of around 2 km. Although theoretical, this value seems in agreement with the size of small events that have been detected in other geothermal fields equipped with dense surface networks. Indeed, catalogs with a magnitude of completeness equal to 0 are currently generated with the seismicity detected in the geothermal site of Landau at 6–8 km of depth (Vasterling et al., 2017); earthquakes with $M \geq -0.6$ and depth of 3 km are present in the catalogue of Rittershoffen geothermal site (Meyer et al., 2017) and at the Habanero and Paralana sites (Australia), where the microseismicity occurs at more than 4 km of depth, earthquakes with $M \geq -0.8$ are located (Riffault et al., 2018). Therefore, we can assume that SENSI algorithm is providing estimations that seem to reflect the real potential sensitivity of the network.

Finally, thanks to the network designed in this manuscript, 10 stations were installed in 2021 and allowed to record the seismic activity associated with the hydraulic stimulation realized to enhance the permeability of the reservoir. 57 events with duration magnitude ranging between −1.6 and −0.5 were recorded during and after an injection of fluids (Figueroa-Soto et al., in submission). Events were mainly located at about 1.2–1.5 km of depth and the epicentral errors were estimated on 0.14 km for most of the induced events (Figueroa-Soto et al., in submission).

6. Data and resources

Seismic noise records used in this study were collected as part of the Work Project 5.2 of GEMex using Trillium Compact post-hole 120 s instruments. More information about the project can be found at www.gemex-h2020.eu. Digital Elevation Model (DEM) was obtained from Mexican National Institute of Statistics and Geography (INEGI) at www.inegi.org.mx/app/geo2/elevacionesmex/. The programs are available upon request from the authors.

CRediT authorship contribution statement

Leonarda I. Esquivel-Mendiola: Writing – original draft, Software, Methodology, Investigation, Formal analysis, Conceptualization. **Marco Calò:** Writing – review & editing, Validation, Supervision, Resources, Methodology, Conceptualization. **Anna Tramelli:** Writing – review & editing, Validation, Supervision, Software, Resources, Methodology, Conceptualization. **Angel Figueroa-Soto:** Writing – review & editing, Validation, Supervision, Resources.

Declaration of competing interest

The authors declare that they have no known competing financial interests or personal relationships that could have appeared to influence the work reported in this paper.

Data availability

Data will be made available on request.

Acknowledgment

This work is performed in the framework of the Mexican European consortium GEMex (Cooperation in Geothermal energy research Europe-Mexico, PT5.2 N: 267084 funded by CONACyT-SENER: S0019, 2015–04, and of the joint agreement between UNAM and INGV on the development of seismological research of volcanic and geothermal field (N:44753-1023-22-IV-16/1).

References

Avellán, D.R., Macías, J.L., Layer, P.W., Sosa-Ceballos, G., Gómez-Vasconcelos, M.G., Cisneros-Máximo, G., Sánchez-Núñez, J.M., Martí, J., García-Tenorio, F., López-Loera, H., Pola, A., Benowitz, J., 2020. Eruptive chronology of the Acoculco caldera complex – a resurgent caldera in the eastern Trans-Mexican Volcanic Belt (México). J. S. Am. Earth Sci. 98 https://doi.org/10.1016/j.jsames.2019.102412. August 2019.

Bartal, Y., Somer, Z., Leonard, G., Steinberg, D.M., Ben Horin, Y., 2000. Optimal seismic networks in Israel in the context of the comprehensive test ban treaty. Bull. Seismol. Soc. Am. 90 (1), 151–165. https://doi.org/10.1785/0119980164.

Baujard, C., Genter, A., Cuenot, N., Mouchot, J., Maurer, V., Hehn, R., Ravier, G., Seibel, O., Vidal, J., 2018. Experience learnt from a successful soft stimulation and operational feedback after 2 years of geothermal power and heat production in rittershoffen and soultz-sous-forêts plants (Alsace, France). Trans. Geoth. Resour. Counc. 42, 2241–2252.

Bolós, X., Del Ángel, V., Villanueva-Estrada, R.E., Sosa-Ceballos, G., Boijseauneau-López, M., Méndez, V., Macías, J.L., 2022. Surface hydrothermal activity controlled by the active structural system in the self-sealing geothermal field of Acoculco (Mexico). Geothermics 101. https://doi.org/10.1016/j.geothermics.2022.102372. August 2021.

Bondár, I., Myers, S., Engdahl, E., Bergman, E., 2004. Epicentre accuracy based on seismic network criteria. Geophys. J. Int. 156 (3), 483–496. https://doi.org/10.1111/j.1365-246X.2004.02070.x.

Brune, J.W., 1970. Tectonic stress and the spectra of the seismic shear waves from earthquakes. J. Geophys. Res. 75 (26), 4997–5009. https://doi.org/10.1029/JB075i026p04997.

Buijze, L., Bijsterveldt, L., Cremer, H., Jaarsma, B., Paap, B., Veldkamp, J.G., Wassing, B., Van Wees, J., van Yperen, G., ter Heege, J., 2019. Induced seismicity in geothermal systems: occurrences worldwide and implications for The Netherlands. In: European Geothermal Congress 2019.

Coles, D., Curtis, A., 2011. Efficient nonlinear Bayesian survey design using DN optimization. Geophysics 76 (2). https://doi.org/10.1190/1.3552645. Q1-Q8.

De Landro, G., Picozzi, M., Adinolfi, G.M., Russo, G., Zollo, A., 2020. Seismic networks layout optimization for a high-resolution monitoring of induced micro-seismicity. J. Seismol. 24, 953–966. https://doi.org/10.1007/s10950-019-09880-9.

D'Alessando, A., Badal, J., D'Anna, G., Papanastasiou, D., Baskoutas, I., Meral Ozel, N., 2013. Location performance and detection threshold of the Spanish national seismic network. Pure Appl. Geophys. 170, 1859–1880. https://doi.org/10.1007/s00024-012-0625-y.

D'Alessando, A., Guerra, I., D'Anna, G., Gervasi, A., Harabaglia, P., Luzio, D., Stellato, G., 2014. Integration of onshore and offshore seismic arrays to study the seismicity of the Calabrian Region: a two steps automatic procedure for the identification of the best stations geometry. ADGEO 36, 69–75. https://doi.org/10.5194/adgeo-36-69-2014.

D'Alessandro, A., Luzio, D., D'Anna, G., Mangano, G., 2011a. Seismic network evaluation through simulation: an application to the Italian national seismic network. Bull. Seismol. Soc. Am. 101 (3), 1213–1232. https://doi.org/10.1785/0120100066.

D'Alessandro, A., Papanastassiou, D., Baskoutas, I., 2011b. Hellenic unified seismological network: an evaluation of its performance through SNES method. Geophys. J. Int. 185 (3), 1417–1430. https://doi.org/10.1111/j.1365-246X.2011.05018.x.

Eberhart-Phillips, D., 1993. Local earthquake tomography: earthquake source regions. In: Hirahara, H.M. Iyer y K. (Ed.), Seismic Tomography: Theory and Practice. Chapman and Hall, London, U. K., pp. 613–643. http://pubs.er.usgs.gov/publication/70186523

Edwards, B., Kraft, T., Cauzzi, C., Kästli, P., Wiemer, S., 2015. Seismic monitoring and analysis of deep geothermal projects in St Gallen and Basel, Switzerland. Geophys. J. Int. 201 (2), 1022–1039. https://doi.org/10.1093/gji/ggv059.

Figueroa-Soto, A., Perton, M., López-Hernández, A., Márquez-Ramírez, V.H., Caló, M., 2022. Induced Seismicity Response of Hydraulic Fracturing in Acoculco, Puebla Mexico: Results of Passive Seismic Monitoring in a Geothermal System in submission.

Gaucher, E., Schoenball, M., Heidbach, O., Zang, A., Fokker, P., Van Wees, J., Kohl, T., 2015. Induced seismicity in geothermal reservoirs: a review of forecasting approaches. Renew. Sustain. Energy Rev. 52, 1473–1490. https://doi.org/10.1016/j.rser.2015.08.026.

GEMex, W.P., 5.2, 7.2 and 7.3. Final Report, 2021. Informe del Procesamiento de Datos Adquiridos durante la prueba de Estimulación de Pozo EAC-1 en la zona Geotérmica de Acoculco. Puebla.

GEMex W.P. 7.1, 2020. Report on Model of Potential Drill Target and Proposed Drill Path.

Guerrero-Martínez, F.J., Prol-Ledesma, R.M., Carrillo-De La Cruz, J.L., Rodríguez-Díaz, A.A., González-Romo, I.A., 2020. A three-dimensional temperature model of the Acoculco caldera complex, Puebla, Mexico, from the Curie isotherm as a boundary condition. Geothermics 86 (September 2019), 101794. https://doi.org/10.1016/j.geothermics.2019.101794.

Gupta, H.K., 1992. Reservoir induced earthquakes. In: Developments in Geotechnical Engineering, vol. 64. Elsevier, ISBN 9780444889065.

Hardt, M., Scherbaum, F., 1994. The design of optimum networks for aftershock recordings. Geophys. J. Int. 117 (3), 716–726. https://doi.org/10.1111/j.1365-246X.1994.tb02464.x.

Ibarra-Bustos, P.D., 2019. Análisis de la criticalidad de la corteza superior y sus relaciones tectónicas con el sistema geotérmico de Acoculco, Puebla, a partir de registros de ruidos sísmico. Tesis de maestría. Universidad Michocana de San Nicolas de Hidalgo. http://bibliotecavirtual.dgb.umich.mx:8083/xmlui/handle/DGB_UMICH/4433.

Kijko, A., 1977. An algorithm for optimum distribution of a regional seismic network-I. PAGE 115, 999–1009. https://doi.org/10.1007/BF00881222.

Kraft, T., Mignan, A., Giardini, D., 2013. Optimization of a large-scale microseismic monitoring network in northern Switzerland. Geophys. J. Int. 195 (1), 474–490. https://doi.org/10.1093/gji/ggt225.

Kruszewski, M., Hofmann, H., Alvarez, F.G., Bianco, C., Haro, A.J., Garduño, V.H., Liotta, D., Trumpy, E., Brogi, A., Wheeler, W., Bastesen, E., Parisio, F., Saenger, E.H., 2021. Integrated stress field estimation and implications for enhanced geothermal system development in Acoculco, Mexico. Geothermics 89, 101931. https://doi.org/10.1016/j.geothermics.2020.101931. July 2020.

Lengliné, O., Lamourette, L., Vivin, L., Cuenot, N., Schmittbuhl, J., 2014. Fluid-induced earthquakes with variable stress drop. J. Geophys. Res. Solid Earth 119 (12), 8900–8913. https://doi.org/10.1002/2014JB011282.

Lermo, J., Antayhua, Y., Bernal, I., Venegas, S., Arredondo, J., 2009. Monitoreo sísmico en la zona geotérmica de Acoculco, Pue., México. Geotermia 22 (1), 40–58.

López-Hernández, A., Castillo-Hernández, D., 1997. Exploratory drilling at Acoculco, Puebla, Mexico: a hydrothermal system with only nonthermal manifestations. Trans. Geoth. Resour. Counc. 21, 429–433.

López-Hernández, A., García-Estrada, G., Aguirre-Díaz, G., González-Partida, E., Palma-Guzmán, H., Quijano-León, J.L., 2009. Hydrothermal activity in the tulancingo-acoculco caldera complex, central Mexico: exploratory studies. Geothermics 38 (3), 279–293. https://doi.org/10.1016/j.geothermics.2009.05.001.

Mahani, A., Kao, H., Walker, D., Johnson, J., Salas, C., 2016. Performance evaluation of the regional seismograph network in northeast British columbia, Canada, for monitoring of induced seismicity. Seismol Res. Lett. 87 (3), 648–660. https://doi.org/10.1785/0220150241.

Maldonado-Hernández, L.T., Perton, M., Figueroa-Soto, A., Caló, M., Jousset, P., 2019. Exploración sísmica de la caldera de Acoculco, Puebla. 2019. In: Annual Meeting of the Mexican Geophysical Union.

Meyer, G., Baujard, C., Hehn, R., Genter, A., Mcclure, M., 2017. Analysis and numerical modelling of pressure drops observed during hydraulic stimulation of GRT-1 geothermal well (rittershoffen, France). In: Proceedings of the 42nd Workshop on Geothermal Reservoir Engineering, 1, p. 14, 1.

Mitchell, T.J., 2000. An algorithm for the construction of "D-optimal" experimental designs. Technometrics 42 (1), 48–54. https://doi.org/10.2307/1271431.

Mukuhira, Y., Asanuma, H., Niitsuma, H., Häring, M.O., 2013. Characteristics of large-magnitude microseismic events recorded during and after stimulation of a geothermal reservoir at Basel, Switzerland. Geothermics 45, 1–17. https://doi.org/10.1016/j.geothermics.2012.07.005.

Myers, S.C., Schultz, C.A., 2000. Improving sparse network seismic location with Bayesian kriging and teleseismically constrained calibration events. Bull. Seismol. Soc. Am. 90 (1), 199–211. https://doi.org/10.1785/0119980171.

Orazi, M., D'Auria, L., Tramelli, A., Buonocunto, C., Capello, M., Caputo, A., De Cesare, W., Giudicepietro, F., Martini, M., Peluso, R., Scarpato, G., 2013. The seismic monitoring network of Mt. Vesuvius. Ann. Geophys. 56 (4). S0450-S0450.

Peterson, J., 1993. Observations and modeling of seismic background noise. U.S. Geol. Survey Open-File Report 93–322. https://doi.org/10.3133/ofr93322.

Rabinowitz, N., Steinberg, D., 1990. Optimal configuration of a seismographic network: a statistical approach. Bull. Seismol. Soc. Am. 80 (1), 187–196. https://doi.org/10.1785/BSSA0800010187.

Rabinowitz, N., Steinberg, D., 2000. A statistical outlook on the problem of seismic network configuration. In: Thurber, C.H., Rabinowitz, N. (Eds.), Advances in Seismic Event Location. Kluwer Academic Publisher, Dordrecht, The Netherlands, pp. 51–69.

Riffault, J., Dempsey, D., Karra, S., Archer, R., 2018. Microseismicity cloud can Be substantially larger than the associated stimulated fracture volume: the case of the Paralana enhanced geothermal system. J. Geophys. Res. Solid Earth 123 (8), 6845–6870. https://doi.org/10.1029/2017JB015299.

Schoenball, M., Kohl, T., 2013. The peculiar shut-in behavior of the well GPK2 at Soultz-sous-Forêts. Trans. Geoth. Resour. Counc. 37, 217–220.

Schoenball, M., Müller, T.M., Müller, B.I.R., Heidbach, O., 2010. Fluid-induced microseismicity in pre-stressed rock masses. Geophys. J. Int. 180 (2), 813–819. https://doi.org/10.1111/j.1365-246X.2009.04443.x.

Stabile, T.A., Iannaccone, G., Zollo, A., Lomax, A., Ferulano, M., Vetri, L., Barzaghi, L., 2013. A comprehensive approach for evaluating network performance in surface and borehole seismic monitoring. Geophys. J. Int. 192 (2), 793–806. https://doi.org/10.1093/gji/ggs049.

Steinberg, D., Rabinowitz, N., 2003. Optimal seismic monitoring for event location with application to on site inspection of the comprehensive nuclear test ban treaty. Metrika 58, 31–57. https://doi.org/10.1007/s001840200222.

Thurber, C.H., 1993. Local earthquake tomography: velocities and Vp/Vs-theory. In: Iyer, H.M., Hirahara, K. (Eds.), Seismic Tomography: Theory and Practice. Chapman and Hall, London, pp. 563–583.

Thurber, C., Eberhart-Phillips, D., 1999. Local earthquake tomography with flexible gridding. Comput. Geosci. 25 (7), 809–818. https://doi.org/10.1016/S0098-3004(99)00007-2.

Toledo, T., Jousset, P., Maurer, H., Krawczyk, C., 2020. Optimized experimental network design for earthquake location problems: applications to geothermal and volcanic field seismic networks. J. Volcanol. Geoth. Res. 391, 106433 https://doi.org/10.1016/j.jvolgeores.2018.08.011.

Tramelli, A., Troise, C., De Natale, G., Orazi, M., 2013. A new method for optimization and testing of Microseismic networks: an application to Campi Flegrei (Southern Italy). Bull. Seismol. Soc. Am. 103 (3), 1679–1691. https://doi.org/10.1785/0120120211.

Tramelli, A., Peluso, R., Orazi, M., Troise, C., Natale, G.D., 2015. A FORTRAN code for the sensitivity estimate of a seismic network: an application to campi flegrei. J. Petrol Environ. Biotechnol. 6 (6), 254. https://doi.org/10.4172/2157-7463.1000254.

Urban, E., Lermo, J., 2017. Fracture and stress evaluation using well logs and microseismicity, in the exploitation of Los Humeros geothermal field, Mexico. Trans. Geoth. Resour. Counc. 41, 1756–1780.

Vasterling, M., Wegler, U., Becker, J., Brüstle, A., Bischoff, M., 2017. Real-time envelope cross-correlation detector: application to induced seismicity in the Insheim and Landau deep geothermal reservoirs. J. Seismol. 21 (1), 193–208. https://doi.org/10.1007/s10950-016-9597-1.